Origins of polysaccharide conformation and viscoelasticity in miscible heterogeneous solvent

Gleb Yakubov (✉ Gleb.Yakubov@nottingham.ac.uk)

University of Nottingham   https://orcid.org/0000-0001-5420-9422

Pallab Kumar Borah

University of Nottingham

Amir Irani

University of Waikato

Joshua Reid

University of Nottingham

Thomas MacCalman

University of Nottingham

Benjamin Westberry

Massey University

Vlad Dinu

University of Nottingham

Philippe Prochasson

Motif FoodWorks Inc.

Michael Boehm

Motif FoodWorks Inc.

Stephen Harding

University of Nottingham   https://orcid.org/0000-0002-7798-9692

Reed Nicholson

Motif FoodWorks Inc.

Martin Williams

Massey University

Stefan Baier

The University of Queensland

Article

Keywords:

Posted Date: November 13th, 2023

DOI: https://doi.org/10.21203/rs.3.rs-3500497/v1

Additional Declarations: There is **NO** Competing Interest.

Origins of polysaccharide conformation and viscoelasticity in miscible heterogeneous solvent

Pallab Kumar Borah[a], Amir H. Irani[b,c], Joshua E. S. J. Reid[a], Thomas MacCalman[d], Benjamin Westberry[e], Vlad Dinu[d], Philippe Prochasson[f], Michael W. Boehm[f], Stephen E. Harding[d], Reed A. Nicholson[f], Martin A. K. Williams[e], Stefan K. Baier[f,g], Gleb E. Yakubov[a]*

[a] *Food and Biomaterials Group, School of Biosciences, University of Nottingham, LE12 5RD, United Kingdom*

[b] *Department of Anaesthesia, Te Whatu Ora, Waikato Hospital, Hamilton 3204, New Zealand*

[c] *School of Engineering, University of Waikato, Hamilton 3240, New Zealand*

[d] *National Centre for Macromolecular Hydrodynamics, School of Biosciences, University of Nottingham, LE12 5RD, United Kingdom*

[e] *School of Fundamental Sciences, Massey University, Palmerston North 4442, New Zealand*

[f] *Motif FoodWorks Inc, 27 Drydock Avenue, Boston, MA 02210, United States of America.*

[g] *School of Chemical Engineering, The University of Queensland, Brisbane, QLD 4072, Australia.*

*Corresponding author:

Gleb E. Yakubov, Associate Professor of Food Physics, Food and Biomaterials Group, School of Biosciences, University of Nottingham, LE12 5RD, United Kingdom.

Polysaccharide polymers constitute the fundamental building blocks of life and display a diverse set of conformational states which results in complex viscoelastic behaviour of their solutions; the origins of which needs further understanding. Utilising a model high molecular weight, high Trouton ratio 'pectin' polysaccharide extracted from okra (*Abelmoschus esculentus*) mucilage, we combine computer simulations and experimental data to unveil the underlying microscopic hydrodynamic origins of polysaccharide conformation. In miscible heterogenous solvents of water and glycerol, the polysaccharide chain undergoes a conformational transition from swelled-to-collapsed configurations, resulting in marked viscoelastic response. The conformational transition is entropy driven. Molecularly adsorbed water molecules have increased presence within ca. 0.40 nm of the chain surface with increase of glycerol in the solvent composition, thus indicating *the emergence of preferential solvation.* This preferential solvation elicits an entropically unfavourable dynamic solvent heterogeneity, which is lessened by swelling and collapse of polysaccharide chains. Altering the preferential solvation layer by adjusting solvent composition allows for precise control of chain conformation and viscoelastic parameters. Our results provide an essential missing piece of the puzzle that is inaccessible through mean-field assumptions and offer new fundamental insights applicable in biological, biomedical, and engineering applications, including microrheological flows, microfluidics, bio-inkjet printing, as well as in pharmacological and food formulations.

Polysaccharides are the most abundant class of natural polymers. Alongside proteins, lipids, and nucleic acids, polysaccharides constitute the fundamental building blocks of life.[1] Polysaccharides are long-chain polymeric carbohydrates composed of monosaccharide units linked together by glycosidic bonds, and exhibit a wide range of structural variations, ranging from linear to highly branched structures. Depending on their specific structure, polysaccharides serve various functions in living organisms, from providing structural integrity to exchanging and processing information. For instance, cellulose and pectin provide structural support in plant cell walls, and chitin forms the exoskeleton of arthropods, whilst highly viscoelastic acidic polysaccharide mucilage facilitates the capture of prey in carnivorous plants.[2-5] Furthermore, polysaccharide chains (polymeric glycans) of the glycocalyx, a carbohydrate-rich layer surrounding cells across all life forms, including bacteria and humans, play a vital role in immunomodulation.[6,7] However, the full significance of polysaccharide conformations in the above and other key biological structures such as enzymes, antibodies, biofilms, and biosurfactants is not yet fully understood.[8-11] This is partly due to the complex three-dimensional conformation of polysaccharides, which determines their interactions and biophysical behaviour.[12,13] Over the past two decades, extensive research has been undertaken to shed light on the conformation of polysaccharides and how this links to their functionality due to their crucial relevance in a wide range of biological functions as mentioned above, and also applications in food science, synthetic plant cells, bioelectronics, biomedical applications, and pharmaceuticals.[14-19]

The complex three-dimensional conformation of polysaccharides in solution, typically water as the solvent, impacts on the manifest hierarchical architectures and viscoelastic properties of their solutions in natural and applied environments. Past theoretical and experimental studies have delved deeper into the influence of parameters such as polysaccharide charge, salt environments, solution pH, and small molecules on polysaccharide

3

65 conformation and solution rheology.[20-26] However, the role of solvent composition and entropic

66 interactions associated with the solvent has been largely unexplored, despite the crucial role of

67 polysaccharide structure and conformation in biological processes.[18] While it is known that

68 water has a considerable influence on polysaccharide or polymer conformation, beyond

69 carefully controlled laboratory experiments, water is seldom pure. Other components, *i.e.*, the

70 cosolvent (referred to as an osmolyte rather commonly in *e.g.*, protein biophysics), can

71 drastically alter behaviour. This is especially true under extreme conditions, including those of

72 low water activity, high salinity or interactions with ice. Indeed, cosolvents, for *e.g.*, glycerol

73 in water is known to modify water activity[27] and water's propensity for self-interaction,[28] and

74 is crucial to life-sustaining phenomena such as the osmoprotection and freeze resistance in fish,

75 plants, and insects.[29-31]

76   Although few studies in miscible solvents (water and polyols/sugars) have shown

77 alterations in conformation and relaxation time in a wide variety of polysaccharides, including

78 pectins[21,32], chitosan,[33] and xanthan,[34] the molecular mechanisms behind these transitions have

79 remained partly elusive. One of the key challenges is the way a miscible solvent is described.

80 The topic of conformational change in 'polymer science' is typically considered based on

81 scaling law predictions that describe how the system free energy, *F(R)* depends on polymer

82 conformation or size, R as, $F(R) = \frac{R^2}{Nb^2} + \frac{B_2 N^2}{R^3} + \frac{B_3 N^3}{R^6}$. This simple one-

83 component mean-field treatment pioneered by Flory and de Gennes[35,36] successfully describes

84 polymer chains swelling in good solvents versus collapse in poor solvents. The problem of this

85 perspective is that any information on the heterogeneity of solvent or co-solvents is lost. A

86 more general approach would be to consider the solvent at a length-scale where heterogeneity

87 is not ignored, *i.e.*, along or around a polymer chain where a miscible solvent can undergo

88 partitioning, a phenomenon often called '*preferential solvation*'. Preferential solvation refers

89 to the distribution of solvent molecules around a solute molecule, which can deviate

90 significantly from the statistical distribution observed in the bulk solution. A rigorous

91 perspective has been provided recently by Mukherji et al.[37,38] using a discrete particle-based

92 approach. The authors describe polymer swelling and collapse in miscible good solvents as

93 well as miscible bad solvents by considering the effect of preferential solvation, a point of view

94 which is contrary to mean-field behaviour.

95   So, why is a new perspective required now? While previous viewpoints provide some

96 important insights, they may fall short in describing polymer behaviour in miscible

97 heterogeneous solvent environments. A description of polymer conformational transitions in

98 miscible heterogenous solvents, especially polymers with complex conformations such as

99 polysaccharides, also remains unclear despite their pivotal significance in biological processes

100 as discussed above. To elucidate the role of composition of a miscible heterogeneous solvent

101 on polysaccharide conformation and viscoelasticity, we utilise a heteropolysaccharide from

102 okra (*Abelmoschus esculentus*) mucilage, called pectin. Pectin is a model natural

103 polysaccharide widely used in foods, pharmaceuticals and environmental engineering (*e.g.*, as

104 a bioflocculant) due to its unique and complex viscoelastic spectrum, and high Trouton

105 ratio.[14,39,40] The polysaccharide also allows measurements of both shear and extensional

106 rheological properties for a wide range of chain conformations, making it ideal for the present

107 study. Briefly, the polysaccharide predominantly comprises, (a) rhamnogalacturonan-I, a

108 bottlebrush-like polymer made up of repeating units of the disaccharide 1,2-α-*l*-rhamnose-1,4-

109 *α-d*-galacturonic acid, with a large number of rhamnose residues linked to linear and branched

110 *β-d*-galactopyranosyl and/or *α-l*-arabinofuranosyl residues, and (b) homogalacturonan, a linear

111 homopolymer of *α*-1,4-linked-*d*-galacturonic acid.[40] Earlier studies have pointed that water is

112 a good solvent for pectin, where the polysaccharide adopts a so-called flexible conformation.[41-

113 43] In our study, we utilise binary water-glycerol mixtures as a miscible heterogenous solvent

114 model, where glycerol acts as an 'inert' cosolvent and could be generally regarded as a 'poor'

115 solvent for polysaccharides.[44,45] For example, dextran in glycerol demonstrates a free energy

116 of interfacial interaction, ΔG_{121} = -2.11; the negative value indicates that glycerol is a poor

117 solvent.[45] Our initial observations also suggested that pectin was insoluble in glycerol ($\geq$

118 99.0%), confirming that glycerol is a poor solvent for pectin. Therefore, in miscible

119 heterogenous solvents of water and glycerol, we hypothesise that an adequate balance of

120 entropically driven interactions based on global solvent composition can be achieved. This sets

121 the scene for understanding the role of solvation in governing polysaccharide conformation

122 and solution viscoelasticity.

Results

Conformation and solvation of polysaccharide chains in solution. We first demonstrate a simple all-atom picture of polysaccharide chain conformation and polysaccharide-solvent interactions by simulating a dodecamer of the pectin polysaccharide chain in binary water-glycerol mixtures. Note, the pectin solutions (pectin in water + glycerol) are denoted as ϕ_0, ϕ_{20}, ϕ_{40}, ϕ_{60} and ϕ_{80} or $\phi_{0\rightarrow80}$ corresponding to $0 \rightarrow 80$ vol.% of aqueous glycerol and are described as such throughout the article. We examined the chain's average radius of gyration, R_g, and average end-to-end distance, $\bar{R}$ (after 100 ns of simulation, far in excess of the equilibration time), as these are clear indicators of conformational change in the chains. In ϕ_0, we observed a chain configuration with R_g and $\bar{R}$, as 1.07 nm and 3.24 nm, respectively (Figure 1a). We postulate that ϕ_0 is the flexible conformation of the polysaccharide in concurrence with earlier studies which suggest that water is a good solvent for pectin, and the polysaccharide adopts a flexible conformation.[41-43] Upon increasing glycerol in our systems, a swelling of chains is evident for $\phi_{20\rightarrow40}$, corroborated by increase in R_g and $\bar{R}$ (Figure 1a). Here, $\bar{R}$ approaches the chain's contour length, $L = Nd \sin{^\theta/_2} = 4.40$ nm, where N is number of units, d is unit length (Rha-GalA disaccharide monomer, ca. 0.90 nm)[46], and θ for C-O-C is 109.5°. However, in $\phi_{60\rightarrow80}$, it appears that the pectin chains undergo shrinkage due to chain folding on itself. We will use the term 'chain collapse' when referring to such configuration to reflect the compounding effect of volumetric changes and the structural folding. The chain collapse is marked by a pronounced decrease in R_g and $\bar{R}$ (Figure 1a). Since ca. 10000 chain conformations were sampled in the 100 ns simulation to derive the average R_g and $\bar{R}$, we extracted the low energy chain conformations in $\phi_{0\rightarrow80}$ from free energy surface analysis by describing the polysaccharide free energy as, $\Delta G(r_{op}) = -k_B T[\ln P(r_{op}) - \ln P_{max}]$, where P is the probability distribution along coordinate r, and P_{max} describes its maxima, which is

147 subtracted to ensure that $\delta G \rightarrow 0$ for the lowest free energy minimum. The order parameter,

148 r_{op}, gives rise to a reweighted free energy surface. Numerically, we evaluated $r_{op} =$

149 $f(RMSD, R_g)$.[47] The respective free energy surfaces and corresponding simulation snapshots

150 of low energy pectin chain conformations are shown in Figure 1b-f and Figure 2a-f,

151 respectively. From the free energy surface analysis, it is clear that in the range of $\phi_{0 \rightarrow 40}$, the

152 chain appears to exhibit flexible and swelled conformations. This is followed by chain collapse

153 in $\phi_{60 \rightarrow 80}$. It is of note that in ϕ_{60}, two low energy areas are observed in Figure 1e. The

154 representative low energy conformations occurring within these minima, are shown in Figure

155 2d, e. It appears that in ϕ_{60}, the two conformations coexist, and the increase in glycerol

156 concentration falls short to cause uniform chain collapse in the conformation ensemble.

157 However, as glycerol increases further in ϕ_{80}, chain collapse is observed in the ensemble, as

158 seen from the occurrence of a single low energy area in Figure 1e. This transition coincides

159 with significant changes in chain conformation shown in Figure 2f, where marked 'kinks' and

160 'loop' starts to form as initial steps towards chain collapse. Physically, the results could be

161 interpreted as a rough representation of chains with constant contour lengths and varying end-

162 to-end distance depending on whether they are swollen or collapsed.

163
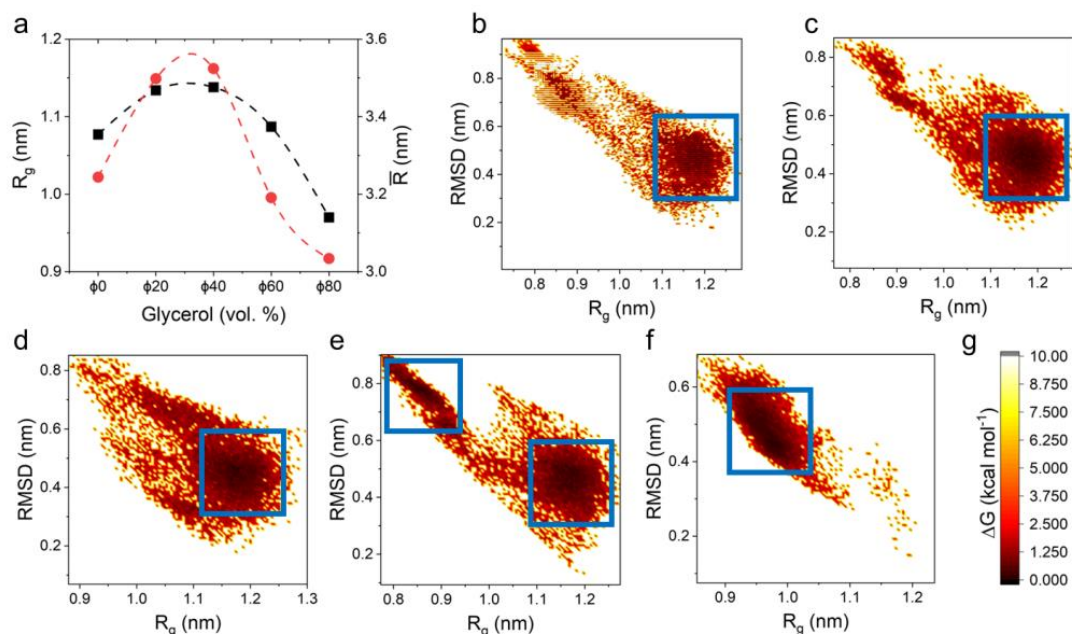
Figure 1. Average radius of gyration, R_g (■) and average end-to-end distance, $\bar{R}$ (●) of polysaccharide chain in $\phi_{0\rightarrow80}$. Black and red dashed lines represent a spline model (a). Free energy surfaces (RMSD as a function of R_g) for polysaccharide chains under infinite dilution are shown as ϕ_0 (b), ϕ_{20} (c), ϕ_{40} (d), ϕ_{60} (e), and ϕ_{80} (f). Blue squares on the free energy surfaces are a visual guide to denote the lowest energy frames. The scalebar shows ΔG of free energy surfaces in kcal mol^{-1} and represented by the colour spectrum, from white to black (g). Simulation time, 100 ns at T = 298 K. Equilibration for all structures was achieved at around 40 - 50 ns of the simulation. RMSD and R_g as a function of simulation time for $\phi_{0\rightarrow80}$ are shown in Figure S1a, b.

173
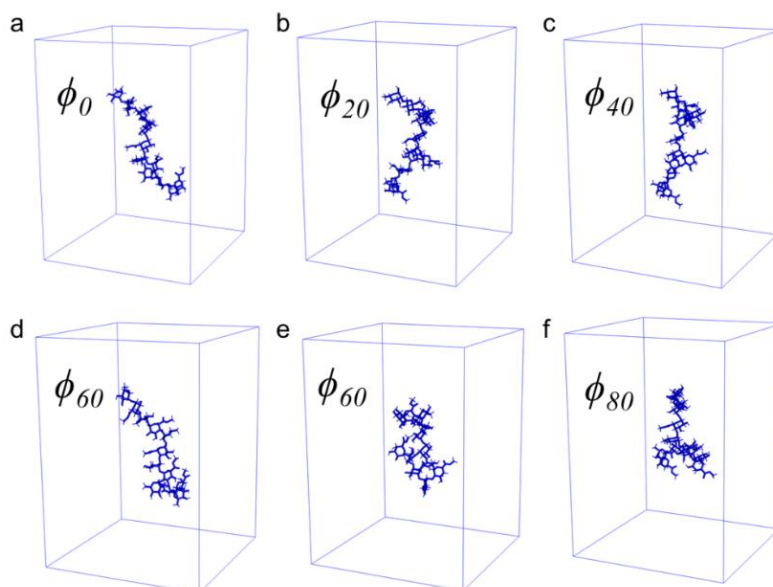
Figure 2. Simulation snapshots showing polysaccharide chain swelling and collapse in ϕ_0 (a), ϕ_{20} (b), ϕ_{40} (c), ϕ_{60} (d), ϕ_{60} (e), and ϕ_{80} (f). (c) and (d) correspond to two different low energy basins observed in ϕ_{60} in Figure 1d. Conformations are drawn from the lowest energy

9

177 frames marked by blue squares in free energy surface shown in Figure 1b-f. Water and glycerol
178 are removed from the periodic box for visual clarity of the chain.

179

180 In good solvents, polymer chains are known to expand, while polymer chains collapse

181 in poor solvents. While the effective monomer-monomer contact in a polymer is repulsive in

182 good solvent and tends to expand the polymer, the interaction is attractive in a bad solvent,

183 leading to chain collapse until restricted by steric packing effects. To probe the solvent

184 contributions which may have led to the observed chain conformations in $\phi_{0\to80}$, the O-O radial

185 probability distribution, $g(r)$ of water and glycerol were probed by considering a pair

186 correlation function $g_{ab}(r)$ between units of a (polysaccharide chain) and b (water, or glycerol)

187 defined as, $g_{ab}(r) = \frac{\langle\rho_b(r)\rangle}{\langle\rho_b\rangle_{local}} = \frac{1}{\langle\rho_b\rangle_{local}} \cdot \frac{1}{N_a} \sum_{i\epsilon a}^{N_a} \sum_{i\epsilon b}^{N_b} \frac{\delta(r_{ij}-r)}{4\pi r^2}$, where $\langle\rho_b(r)\rangle$ represents water

188 or glycerol occurrence at distance r from the polysaccharide chain.[48] Figure 3a, b shows the

189 probability distribution, $g_{ab}(r)$, as a function of radial distance around the chain axis,

190 r. Examination of the solvation shell structure revealed a distinct localisation of water

191 molecules in the proximity of the polysaccharide chain. This implies that the likelihood of

192 water molecules being present in the layer directly adjacent to the polysaccharide chain is much

193 greater, despite the overall increase of glycerol in the system. Notably, as global water fraction

194 decreased in $\phi_{0\to80}$, firstly, a decrease in $g(r)$ is observed for ϕ_{20}, followed by an increase in

195 $g(r)$ of water for $\phi_{40\to80}$ at spatial range r, ca. 0.40 nm (r, distance to first minimum, marked

196 by dashed line in Figure 3a). Here, r, ca. 0.40 nm is thought to correspond to the extent of the

197 first solvation shell, with a $g(r)$ maxima at 0.28 nm which is exactly the nearest-neighbour O-

198 O distance in water.[49] We note, the r-position of the $g(r)$ maxima stays constant throughout

199 $\phi_{0\to80}$ despite the increase in $g(r)$, suggesting water coordination with the monomers of the

200 polysaccharide chain. This coordination could be interpreted as a molecularly adsorbed water

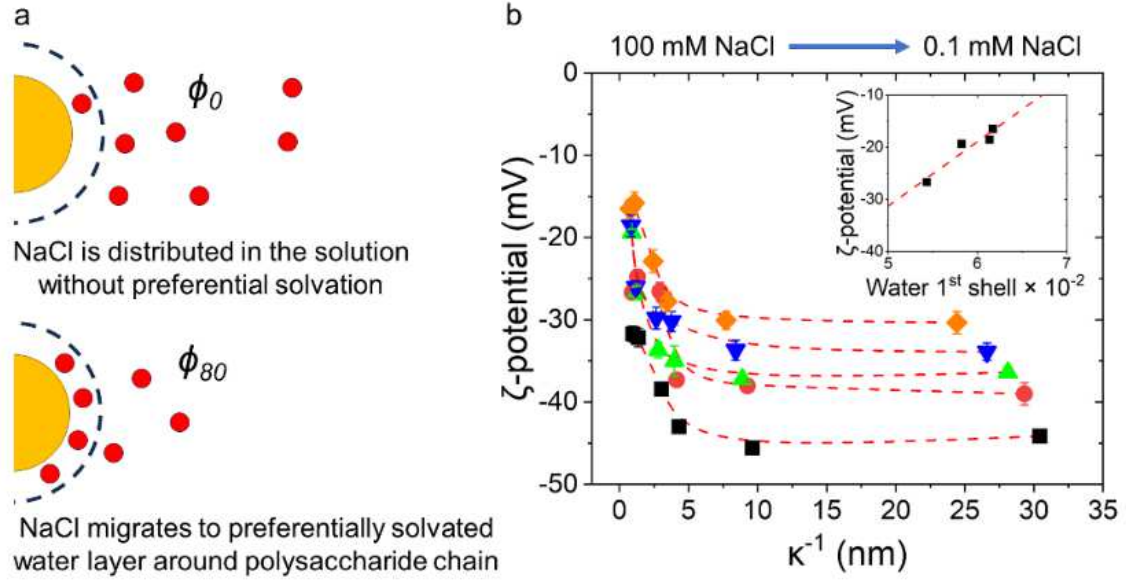201 layer at the polysaccharide-solvent interface (note, these water molecules are still dynamic,

202 albeit with a reduced correlation time, and in exchange with molecules in the unperturbed

10

203 bulk). In addition, examining the glycerol solvation shell, we find its first maxima at r, ca. 0.60

204 nm from the polysaccharide-solvent interface (r, distance to minima, marked by dashed line in

205 Figure 3b). The observed distance, r, for glycerol agrees well with reported data for the nearest-

206 neighbour distance of 0.60 nm for pure glycerol.[50] As the glycerol volume fraction increases,

207 a decrease in $g(r)$ for glycerol at r, 0.60 nm is observed, which coincides with the gradual

208 increase in the probability of water being located in the first solvation shell. This is in

209 agreement with the preferential solvation model proposed by Mukherji et al.[37] and reveals a

210 preferentially solvated layer of water-rich solvent at the polysaccharide-solvent interface. It is

211 worth noting that the solvent accessible surface area (SASA) showed only ca. 2% average

212 relative standard deviation amidst all the conditions probed (Figure 3c). This means that the

213 total chain surface area with water contact was somewhat conserved throughout $\phi_{0\to80}$, and is

214 ameliorated *via* the swelling-collapse transitions of the chains.
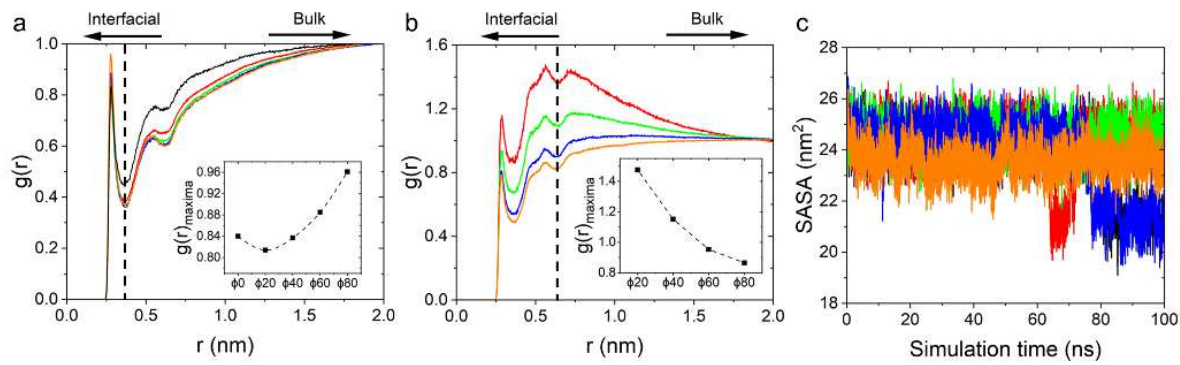
215

216 **Figure 3.** O-O radial distribution function, $g(r)$ as a function of r distance for water (a) and
217 glycerol (b) around polysaccharide chain axis. Black dashed lines are a visual guide to denote
218 the first maximum solvation shell of water and glycerol around the polysaccharide chains.
219 Insets show the $g(r)$ maxima for water and glycerol as a function of solvent composition in
220 $\phi_{0\to80}$. Solvent accessible surface area (SASA) of polysaccharide chains as a function of time
221 (c). Polysaccharide solutions are indicated as, ϕ_0, black; ϕ_{20}, red; ϕ_{40}, green; ϕ_{60}, blue; and ϕ_{80},
222 orange.

Figure 4. Illustration depicting uniform distribution of the electrolyte probe, NaCl (red spheres) in ϕ_0 without preferential solvation effects at the polysaccharide (coloured in yellow)-solvent interface, versus the higher localisation of the electrolyte in the '*water-rich*' solvation shell at the polysaccharide-solvent interface, rather than in the '*water-deficient*' bulk solvent in ϕ_{80}. Dashed lines around polysaccharide indicates the distance of r, 0.40 nm (a). ζ-potential of $\phi_{0 \to 80}$ as a function of Debye length, κ^{-1} (c, 0.01 wt.%). Here, NaCl ranges from 100 to 0.1 mM (left to right). Legends indicate ϕ_0, ■; ϕ_{20}, ●; ϕ_{40}, ▲; ϕ_{60}, ▼; and ϕ_{80}, ♦. Red dashed lines are spline models. Inset shows the linear relationship of ζ-potential in $\phi_{20 \to 80}$ (0.1 mM NaCl) as a function of normalised water in 1st solvation shell (b).

We now provide experimental evidence to the computed $g(r)$ by probing the ζ-potential and electrolyte migration effects as a function of Debye length, κ^{-1} in $\phi_{0 \to 80}$. NaCl was used as a simple electrolyte probe, as NaCl solubility in water > glycerol, *i.e.*, 0.36 g g^{-1} in pure water > 0.08 g g^{-1} in glycerol at 25 °C. The postulate was that the electrolyte probe would uniformly distribute in the solution without preferential solvation, whereas, in the case of preferential solvation, the electrolyte would localise in the '*water-rich*' solvation shell at the polysaccharide-solvent interface, rather than in the '*water-deficient*' bulk solvent (illustrated in Figure 4a). The ζ-potential values were estimated from the measured electrophoretic mobility using the Henry's approximation as, $\mu = \frac{2\epsilon_r \epsilon_0}{3\eta} \zeta f(k_\alpha)$, where ζ is ζ-potential, κ is inverse Debye screening length, α is particle radius, and η is solvent viscosity. Debye screening

12

244 lengths were calculated as, $\kappa^{-1} = \sqrt{\epsilon_r \epsilon_0 k_B T / 2e^2 I}$, where I is electrolyte ionic strength, ε_0 is

245 free space permittivity, k_B is the Boltzmann constant, ε_r is dielectric permittivity, T is absolute

246 temperature, and e is elementary charge. In Figure 4b, we can observe a monotonic decreased

247 in the ζ-potential in $\phi_{0\to80}$ (the values become less negative). Note, the ζ-potential derived from

248 electrophoretic mobility is independent of solvent viscosity as described in the Henry's

249 approximation. Therefore, this result is consistent with the higher degree of ionic localisation

250 at the polysaccharide-solvent interface, and not an artefact arising from solvent viscosity

251 effects. Here, the preferential solvation of water at the polysaccharide-solvent interface

252 facilitates an increase in ionic localisation leading to electrostatic shielding of the

253 polysaccharide chain and shifts the slipping plane closer to the polysaccharide surface. This in

254 turn reduced the electrophoretic mobility of the chains and shows that the magnitude of the ζ-

255 potential has progressively decreased in the $\phi_{0\to80}$. Note, the decrease in ζ-potential for $\phi_{0\to20}$

256 is an effect of NaCl addition and not a direct result of preferential solvation and should be

257 considered with precaution.

258 To probe the preferential solvation effect further, we additionally calculated the number

259 of water molecules at a distance of r, 0.40 nm of the polysaccharide chain from the simulations

260 and normalised it based on the respective number of water molecules in the $\phi_{0\to80}$ systems (the

261 number of water molecule in $\phi_{0\to80}$ simulations is shown in Table S2). Upon observing the

262 relationship between ζ-potential as a function of water in the first solvation shell, we uncovered

263 a linear scaling (Figure 4b, inset). The good agreement with experimental results suggests that

264 indeed the all-atom simulations captured the water localisation around the polysaccharide

265 chains and that this preferential solvation is responsible for the observed changes in ζ-potential.

266 **Viscoelasticity of polysaccharide solutions.** The key consequence of the preferential

267 solvation effect is its impact on the conformation of the polysaccharide chains: either swelling

13

268 or collapse of the chains. Such chain conformations directly influence the properties of

269 polysaccharides in solutions, especially their viscoelastic behaviour. Here we examine how

270 preferential solvation influences polysaccharide viscoelastic properties under conditions of

271 shear and extensional flows. To contextualise observations of viscoelastic behaviour within the

272 framework of polymer solution models, we determined the polymer overlap concentration, c^*,

273 and the entanglement concentration, c_e. The specific viscosity, $\eta_{sp} = {(\eta_0 - \eta_s)}/{\eta_s}$ was

274 measured to establish the limits of dilute-to-entangled regimes in the polysaccharide solutions

275 (η_0 is the zero-shear viscosity and η_s is the solvent viscosity). This enables separating the

276 viscoelastic response of hydrodynamically-independent chains, without the contribution

277 associated with chain interactions and geometric entanglements. The data suggested two

278 regimes as a function of polysaccharide concentration, c in $\phi_{0 \to 80}$, where c^* is approximated

279 to be ca. ≥ 0.01 wt.%, and $c_e > c^*$, as shown in Figure 5a (Regime-I < c^* < Regime-II). Here,

280 the scaling in Regime-I implies $\eta_{sp} \propto c^{1/2}$, $c^{3/2}$, $c^{3/2}$, and $c^{1/2}$, corresponding to $\phi_{0 \to 60}$,

281 respectively (note, scaling for ϕ_{80} was not detected in Regime-I). The scaling in Regime-II

282 broadly implies $\eta_{sp} \propto c^{3/2}$, corresponding to $\phi_{0 \to 80}$. In Regime-I and -II, Fuoss law describes

283 the $c^{1/2}$ scaling and is characteristic behaviour for semi-dilute, unentangled solutions of

284 polysaccharides and for semi-dilute unentangled combs, whereas, $c^{3/2}$ scaling matches the

285 scaling theory prediction for entangled solutions of polysaccharide combs with entangled

286 backbones and unentangled side chains.[22]

287   In the dilute regime, *i.e.*, c < c^*, we probed the hydrodynamic size of scatterers in the

288 $\phi_{0 \to 80}$ systems. The hydrodynamic diameter distribution and the mean hydrodynamic

289 diameter, D_h of the samples are shown in Figure 5b. We observed that the D_h for ϕ_0,

290 780.45 ± 20.65 nm increases in ϕ_{20} to 840.95 ± 34.11 nm and ϕ_{40} to 846.25 ± 3.35 nm with an

291 increase in glycerol in the systems. This was followed by a decline in ϕ_{60} to 648.50 ± 24.20 nm

292   and ϕ_{80} to 467.13 ± 6.81 nm. It is clear that the changing solvent environment resulted firstly

293   in the swelling of the polysaccharide chains thereby increasing the D_h, followed by chain

294   collapse and a dramatic decrease in the D_h, just as observed in the all-atom simulations. In this

295   context, our investigations of infinitely diluted polysaccharide in ϕ_0 using size-exclusion

296   chromatography coupled multi-angle light scattering, SEC-MALS, revealed a molar mass of

297   1.15×10^7 g mol^{-1} for ca. 70% of the polysaccharide chains in the solution (Table S3 and Figure

298   S5a, b). Based on this, we also uncovered a persistence length, l_p of 8.3 nm, and a Mark-

299   Houwink-Sakurada coefficient, $[\eta] = KM_w{}^a$, where a is ca. 0.80; the latter indicates that water

300   is a good solvent for our polysaccharides (Figure 5c, 5c inset). This is consistent with earlier

301   studies that have pointed out that water is a good solvent for pectin.[41-43] Note, SEC-MALS and

302   related data analyses are described in Section S1. Using an average molecular mass of a Rha-

303   GalA disaccharide, 322 g mol^{-1} and a unit length of a Rha-GalA disaccharide monomer, $d =$

304   ca. 0.90 nm,[46] it is now possible to estimate the contour length, L of our polysaccharide chains

305   to 3.21×10^4 nm. Based on this, describing our polysaccharide as a Kratky–Porod chain, a

306   solution to wormlike chain model,[51] $\langle R_g^2 \rangle = {\langle R^2 \rangle}/{6} = \frac{L}{l_p} - \frac{1}{2(l_p)^2}\left(1 - e^{-2l_pL}\right)$ and considering

307   the results from the renormalization group theory for self-avoiding chains,[52] ${R_g}/{r_h} \approx \sqrt{{5}/{2}}$

308   finally gives a prediction for the hydrodynamic size, $2r_h \approx D_h$ of ca. 810 nm, which is in

309   excellent agreement with our D_h estimation of ca. 780 nm for ϕ_0. The agreement between SEC-

310   MALS and D_h provides strong evidence that the scatterers in the dynamic light scattering

311   measurements represent hydrodynamically independent chains, and hence any effect of

312   molecular aggregation can be largely excluded from consideration, as we have tacitly assumed.

313   Therefore, the solvent-induced conformation change occurs within single polymer chains.

314   These findings are further validated by performing intrinsic viscosity, $[\eta]$

315   measurements using capillary viscometry, where $c^*[\eta]$ for ϕ_0 was observed to be ca. 18 dL g$^-$

316   [1]. $c^*[\eta]$ increased in $\phi_{20\rightarrow40}$ to ca. 114 and 140 dL g^{-1}, respectively, and was followed by a

317   decline to ca. 14 and 13 dL g^{-1} in $\phi_{60\rightarrow80}$, respectively (Figure S4b, c). Since, intrinsic viscosity

318   depends on the conformation, flexibility and volume of the polymer, one can connect this

319   observation to a larger pervaded volume of swelled polysaccharide chains which increase the

320   intrinsic viscosity by roughly an order of magnitude in $\phi_{20\rightarrow40}$, as compared to ϕ_0. Conversely,

321   in $\phi_{60\rightarrow80}$, the intrinsic viscosity decreases dramatically, implying a smaller pervaded volume

322   by collapsed chains and compares well with earlier observations in collapsed cellulose gum

323   chains.[22]

324
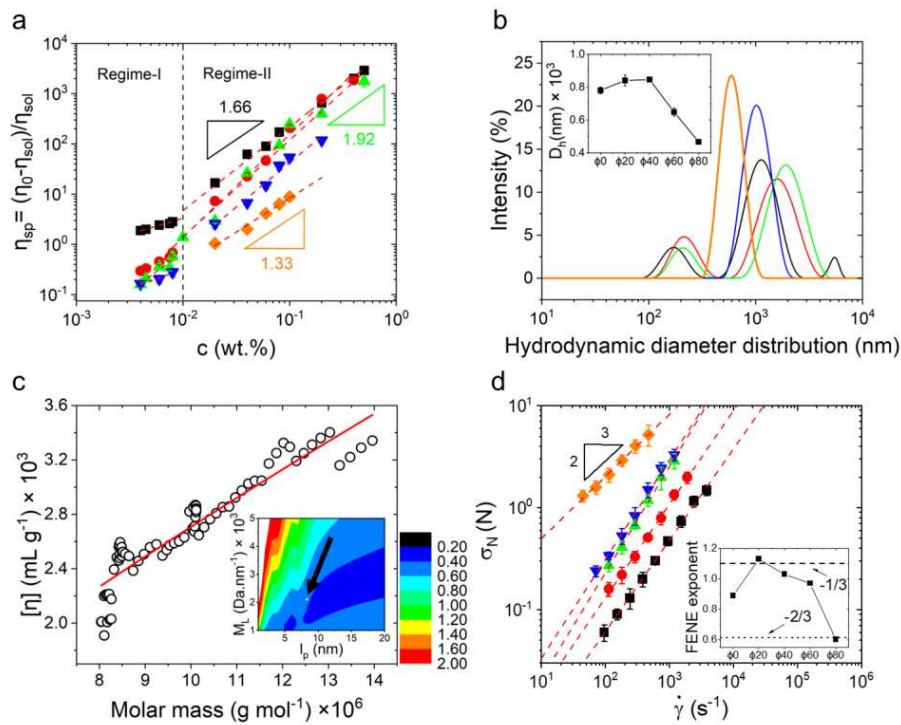
Figure 5. Specific viscosity, η_{sp} of $\phi_{0\rightarrow80}$ as a function of the polysaccharide concentration, c
at 25 °C. Red dashed lines show Power law model fits. Black dashed line is a visual guide to
demarcate the boundaries of Regime-I and -II. Shear viscosity (η) as a function of shear rate
($\dot{\gamma}$) and shear stress (τ) as a function of shear rate ($\dot{\gamma}$) for $\phi_{0\rightarrow80}$ are shown in Figure S2, S3 (a).
Intensity as a function of hydrodynamic diameter distribution for ϕ_0, black; ϕ_{20}, red; ϕ_{40}, green;
ϕ_{60}, blue; and ϕ_{80}, orange at 25 °C (c, 0.001 wt.%). Inset shows the mean hydrodynamic
diameter, D_h (■) as a function of $\phi_{0\rightarrow80}$ (b). Intrinsic viscosity, [η] as a function of molar mass,
shows Mark-Houwink-Sakurada fitting on the M_w, 1.1×10^7 g mol^{-1} polysaccharide fraction
(ca. 70% abundance). Red line indicates Power law model fit. Inset shows contour plot for the
solutions to Bushin–Bohdanecky and Yamakawa–Fujii equations using equivalent radii
approach showing mass per unit length, M_L as a function of persistence length, l_p. The target

336 function, Δ calculated over a range of M_L and l_p, are represented by the full colour spectrum,
337 from black to red. The calculated minimum is indicated as ○ and pointed to with a black arrow
338 (c). FENE description of normal stress (σ_N) as a function of shear rate ($\dot{\gamma}$) in c, 0.5 wt.% okra
339 pectin solutions. Red dashed lines show Power law model fits. Inset show FENE coefficient as
340 a function of $\phi_{0\rightarrow80}$ (d). Legends indicate ϕ_0, ■; ϕ_{20}, ●; ϕ_{40}, ▲; ϕ_{60}, ▼; and ϕ_{80}, ♦.

341

342   In the entangled regimes, *i.e.*, $c_e = c > c^*$, normal stress, σ_N at high shear rate, $\dot{\gamma}$ arising

343 from the Weissenberg effect, $W_i = \dot{\gamma} \cdot \lambda$, gave us a measure of polysaccharide resistance to

344 stretching. A finite extensibility results from the saturation of the stress caused by excessively

345 stretched and orientated polymers, and to understand this, we utilised the FENE-Fraenkel

346 spring-rod approximation[53] which shows a $-\frac{2}{3}$ scaling in viscosity with shear rate for

347 springs, while an adequately rigid and rod-like chain shows a $-\frac{1}{3}$ scaling. A natural way to

348 compare these approximations of 'spring' and 'rod' with a swelled and collapsed chain

349 conformations, is to consider the scaling range where α is the relaxed spring length and δQ is

350 the change in spring length. Assuming this condition, chain configures from a flexible

351 conformation in ϕ_0 (α in thermodynamically good solvent) to a swelled configuration in $\phi_{20\rightarrow40}$

352 ($\alpha + \delta Q$, represents maximum fractional extension closer to contour length), and reverts to a

353 collapsed conformation in $\phi_{60\rightarrow80}$ ($\alpha - \delta Q$, represents maximum fractional collapse). Note,

354 chain cannot collapse to $\delta Q < 0$, and the collapse is limited by steric packing effects. In the

355 normal stress profile, this translates to, t_{zz} (normal stress) $= -\frac{1}{2} \Psi \cdot x^2$, where Ψ is the

356 normal stress coefficient and x is the velocity gradient in fluid.[54] Therefore, in the normal stress

357 profile $-\frac{1}{3}$ dependence with shear rate should correspond to swelled polymers, conversely

358 $-\frac{2}{3}$ corresponds to collapsed polymers. Our results correspond closely to a transition from

359 $-\frac{1}{3}$ and $-\frac{2}{3}$ Power law scaling with FENE exponent of 0.89, 1.13, 1.03, 0.97 and 0.55 in

360 $\phi_{0\rightarrow80}$, respectively, clearly indicating the swelled-to-collapsed transitions in the

polysaccharide chains (Figure 5d). Corresponding Power law scaling in the shear viscosity (η)

362 as a function of shear rate ($\dot{\gamma}$) are shown in Figure S4a.
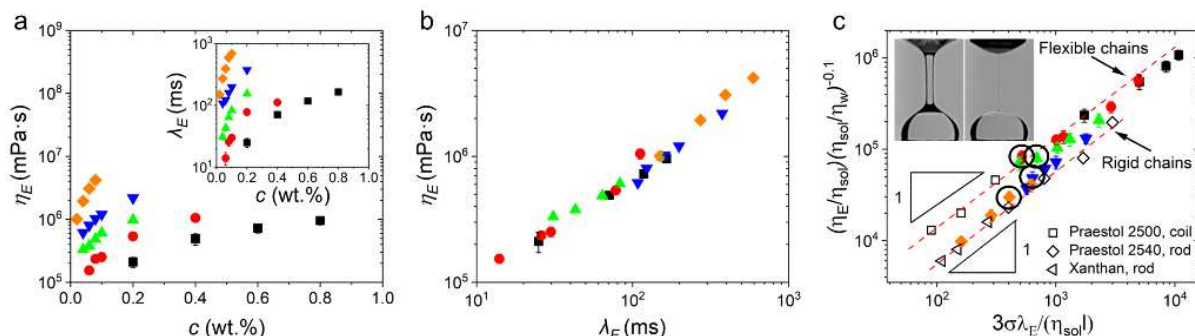
363

Figure 6. Steady-state extensional viscosity, η_E as a function of the polysaccharide concentration, c in okra pectin solutions, $\phi_{0\rightarrow80}$. Inset shows extensional relaxation time, λ_E as a function of the polysaccharide concentration, c in $\phi_{0\rightarrow80}$. The abscissa represents the corresponding values of η_E derived from the linear fit to the filament thinning data, and λ_E are derived from the exponential fit to the filament thinning data. The cut-off for filament thinning was 10 µm in all cases, however filaments endure for longer periods of time than are represented by the filament thinning data utilised for fitting. The machine data for thinning of normalised filament diameter, surface tensions and density required in relation to the calculations are shown in Figure S6, S7. (a). η_E as a function of λ_E (b). Dimensionless η_E as a function of dimensionless λ_E alongside concentration-dependent variation in $\phi_{0\rightarrow80}$ during filament thinning. Here, η_{sol}, η_w, σ, and l are shear viscosity of solvent, shear viscosity of water, surface tension of solution, and filament length, respectively. The dashed red lines correspond to flexible and rigid polysaccharides as described by Stelter and coworkers.[55] Data for praestol (2500 and 2540) and xanthan solutions are renditions of the original figure from Stelter and coworkers.[55] Inset images illustrate the initial exponential conical thinning followed by a linear cylindrical thinning in the late stage for ϕ_{40} during capillary breakup extensional rheology. Black circles indicate the data points for c, 0.06 wt.% polysaccharide solutions (c). Legends in (a), (b), and (c) indicate ϕ_0, ■; ϕ_{20}, ●; ϕ_{40}, ▲; ϕ_{60}, ▼; and ϕ_{80}, ♦. Okra pectin concentration ranges were ϕ_0, 0.2 – 0.8 wt.%; ϕ_{20}, 0.06 – 0.4 wt.%; ϕ_{40}, 0.04 – 0.2 wt.%; ϕ_{60}, 0.04 – 0.2 wt.%; and ϕ_{80}, 0.02 – 0.08 wt.%.

384

385   We also probed the concentration-dependent extensional viscosity, η_E, and the

386 extensional relaxation time, λ_E in $\phi_{0\rightarrow80}$ solution, undergoing capillary thinning and breakup

387 during uniaxial extensional flow, using capillary breakup extensional rheology. Note, capillary

388 thinning was derived from the normalised capillary diameter (d/d_0) undergoing relaxation.

389 The extensional relaxation time, λ_E and the extensional viscosity, η_E were determined from the

390 exponential (at the initial stages of capillary thinning) and linear (at the later stages of capillary

391   thinning) regions as, $D(t) = D_o exp\left(-\frac{t}{3\lambda}\right)$ and $\eta_E = -\frac{\sigma_s}{dD(t)/dt}$, where, D is the diameter of

392   the thinning capillary, D_0 is the diameter of the thinning capillary at time, $t = 0$, and σ_s is the

393   surface tension of the polysaccharide solutions.[55] Figure 6a shows the η_E and λ_E as a function

394   of polysaccharide concentration. Since η_E is governed by λ_E, we probed the η_E/λ_E dependency

395   (Figure 6b). Here, one would quickly recognise that this dependency is accompanied by solvent

396   contributions to viscosity. To remove solvent contributions, η_E and λ_E were rendered

397   dimensionless as described earlier.[55] This led to two η_E/λ_E dependencies, both with $\eta_E \propto \lambda_E$

398   scaling ≈ 1 (Figure 6c). Here, $\phi_{0\to40}$ follow a primary dependency, whilst $\phi_{60\to80}$ follows a

399   secondary dependency. Stelter and coworkers,[55] describes the primary dependencies towards

400   flexible polymer behaviour, whilst the secondary dependency is considered to arise from rigid

401   polymers. Additionally, the comparison of the dependencies observed in our systems with

402   those found in praestol 2500 flexible chains, and praestol 2540 and xanthan with rigid chains

403   from earlier studies,[55] confirm our results. Translating our findings from conformation to

404   viscoelastic responses, the η_E can therefore be described as a manifestation of the contribution

405   of swelled or collapsed polysaccharides to bulk stress. A chain of length $2L$ will contribute

406   equally to bulk stress as that by a rigid sphere of radius L in pure strain state,[56] therefore, as L

407   gets smaller, the contribution to bulk stress goes down. Note, our capillary breakup extensional

408   rheology is essentially a measure of relaxation. Here, we would like to draw attention to the

409   dimensionless λ_E for c, 0.06 wt.% polysaccharide solutions, $\phi_{20\to80}$ (Figure 6c, the data points

410   are encircled by black circles for visual clarity). In swelled polysaccharides, $\phi_{20\to40}$ chains

411   exhibits 'slow' chain relaxation contributing to a longer lifetime of the chain existing in the

412   state of the larger pervaded volume. By contrast, the $\phi_{60\to80}$ systems exhibit 'fast' chain

413   relaxation, contributing to minimising the time the chain occupies a larger pervaded volume.

414   **Discussion**

We now discuss the mechanisms behind the transitions between flexible and collapsed polysaccharide conformations in the miscible heterogenous solvents of water and glycerol; transitions which are key in dictating the biophysical properties of polysaccharide solutions, such as viscoelasticity, in natural and applied environments. First, we consider the case of preferential solvation, a well-known phenomenon, clearly displayed in our all-atom simulations and backed up by our ζ-potential measurements. Consider a polysaccharide chain is introduced at infinite dilution into our two-component solvent mixture of water and glycerol. Here, according to Gibbs's phase rule the number of phases, p relates to the degree of freedom as, $f = 4 - p$.[57] In this case, if composition is dependent and two thermodynamic parameters are independently changeable, $f = 2$ (temperature and pressure), then by phase rule, $p = 2$. The solvent mixture thus separates into two phases, *i.e.*, *preferential solvation*. Next, we hypothesise that swelling-collapse conformational transition of polysaccharide chains are in fact induced by the preferential solvation. A putative mechanism for the swelling-collapse transitions can now be proposed which is rooted in totally non-specific interactions between the polysaccharide chain and solvent. In the first instance, *i.e.*, $\phi_{0 \to 20}$, the radial probability distribution of water decreases in the vicinity of the polysaccharide-solvent interface. Notably, the self-preference of water increases 'exponentially' with addition of glycerol until reaching a maxima near $water_{0.75}/glycerol_{0.25}$ mole fractions (roughly corresponding to ϕ_{40}), which is then followed by an exponential decay of water's self-preference.[28] This water-water self-preference partly explains the decrease in *g(r)* of water at $\phi_{20 \to 40}$, in turn reducing the relative cost of inserting glycerol molecules into the first solvation shell. This sets the scene where glycerol has the steric space to fill the first local solvation shell, thereby preserving the density of the total solvent to the first order (please compare $\phi_{20 \to 40}$ in Figure 3a and b). As a result, in $\phi_{20 \to 40}$, the polysaccharide is now 'somewhat' depleted of water interactions. Under these conditions, the polysaccharide swells and can be interpreted as the system gaining entropy by

440   increasing the area of polysaccharide-water contact through chain swelling. Contrarily, with

441   further increase of glycerol in $\phi_{60\to80}$, water solvation at the interface increases and now

442   glycerol is sterically excluded from the chain locality. Now the system loses entropy by

443   decreasing the area of polysaccharide-water contact through enhancement of chain self-

444   association, leading to the observed collapsed configurations in $\phi_{60\to80}$. Here, the

445   polysaccharide sub-system loses entropy, but water sub-systems gain entropy. The total

446   entropy of the system does increase, leading to the thermodynamic favourability for greater

447   chain collapse. Further experiments are undoubtedly required to clarify this further and

448   consideration of theories *e.g.*, Kirkwood-Buff theory that links macroscopic properties to

449   microscopic details, as well as caveats around specific chain chemistry including side chains

450   and linkage are ongoing and will be part of a future study.

451   We summarise that solvent-solvent and solute-solvent entropic components delicately

452   balance out the total system potential and drives the phenomenon. It is notable that even though

453   our simulations are independent of experimental polysaccharide chain length as well as side-

454   chain characteristics, our simulations demonstrate consensus with our experimental

455   observations. Our data is also in excellent agreement with recently published results on

456   polysaccharide conformation, where addition of glycerol at lower vol. % to aqueous alginate[58]

457   solutions resulted in increased chain flexibility, and, addition of glycerol at higher vol. % to

458   aqueous methylcellulose gum,[59] dextran[60] and hydroxyethyl cellulose[61] solutions resulted in

459   polysaccharide chain collapse. It thus implies that the emergence of our polysaccharide

460   conformations in miscible heterogenous solvent is a generic behaviour whose universal nature

461   ought to be recognised. Our findings provide crucial insight into the role of polysaccharide-

462   water preferential interactions being dominant in miscible heterogenous solvents and points

463   out the resulting implications for governing the conformation and viscoelasticity of

464   polysaccharide solutions. This crucial finding, concealed from prior perspectives, illuminates

465　the role of solvent composition in structural significance of polysaccharides, while

466　simultaneously charting new frontiers in the precise manipulation of polysaccharide

467　conformation and solution viscoelasticity. This applies within both fundamental and practical

468　settings, such as capillary-driven extension and longer-lived viscoelastic filaments, stickiness

469　of carnivorous plant fluids and mammalian saliva, swallowing, extrusion, fibre spinnability,

470　ink jetting, spraying, and emulsion-to-droplet formation. This novel paradigm emerges through

471　the simple yet rational modification of the preferential solvation layer *via* careful tuning of

472　solvent composition and can have exciting implications for the future.

Methods

Materials. Okra fruit was procured from suppliers in Honduras and the polysaccharide, pectin was extracted by hot water extraction as described earlier by Yuan and coworkers[39] with few modifications. Briefly, the fruits (moisture content, 88.42 ± 0.34 %) were cut into ca. 5 mm-thick slices and stirred in water at 55 °C for 90 min (1:10 volume ratio by dry weight basis, solution pH 6.4). The extract was then centrifuged at 8000 g for 30 mins to remove any insoluble cellulosic oligomers and dialyzed (MWCO 10 kDa or 10^4 g mol^{-1}) against 10 volumes of water for 24 h at 4 °C, with three water changes. The material was 10x condensed on a rotary evaporator at 55 °C under vacuum. The resulting viscous liquid was snap frozen in an ethanol-dry ice bath and then lyophilized for further use. The estimations of weight average molar masses (M_w) and monosaccharide composition of the polysaccharide were carried out using Size Exclusion Chromatography coupled to Multiangle Laser Light Scattering (SEC-MALS) and High-Performance Anion Exchange Chromatography with Pulsed Amperometric Detection (HPAEC-PAD), respectively, and are discussed in Section S1, S2, and Figure S5a, b. Degree of methylation was uncovered to be ca. 85%, and was estimated from infrared spectra (4500-700 cm^{-1}) of the polysaccharide obtained on a ATR-FTIR spectrometer (Bruker Optics GmbH, Germany) as described earlier,[62] and results agrees with previous reports.[63]

Glycerol ($\geq$ 99.0%), ethanol, sodium azide, sodium chloride, sodium hydroxide, sodium acetate, *d*-galacturonic acid, *d*-fructose, *d*-mannose, *l*-rhamnose, *l*-arabinose, *d*-galactose, *d*-glucose, *d*-xylose, sulphuric acid, and trifluoroacetic acid were purchased from Sigma-Aldrich, UK. Milli-Q water (Millipore Corp., USA) was used throughout the experiments (18.2 MΩ.cm ionic purity at 25 °C). All experiments were carried out at 25 °C.

Pectin solution preparation. In order to ensure homogenous mixing and prevent polysaccharide chain scission from excessive shear deformation which are known to occur in

497 polymers with high extensibility,[64] the freeze-dried polysaccharide was introduced in water and

498 then placed on a roller for 12 hours. Following this, glycerol at 0, 20, 40, 60 and 80 vol.% was

499 added to the solution and then placed on a roller for another 12 h. Note, 0, 20, 40, 60 and 80

500 vol.% of glycerol equates to ca. 0, 0.06, 0.14, 0.27, 0.50 in mole fractions. Sodium azide was

501 added as an antimicrobial, 0.01% (w/v).

502 **Steady shear rheology and normal stress analysis.** The shear rheology response of

503 polysaccharide solutions were characterised on a MCR 301 rotational rheometer with a Peltier

504 temperature control system (Anton Paar, Austria), using (a) a sandblasted parallel-plate

505 geometry (plate diameter, 40 mm; gap, 100 μm, employed with gap error corrections during

506 data analysis as described previously[65]) or, (b) a concentric cylinder Couette cell geometry for

507 low-viscosity solutions ($\eta_0 \leq 10$ mPa·s). Measurements ($n = 3$) were carried out on shear rate

508 ($\dot{\gamma}$) controlled mode of 10^{-1} to 10^{3} s^{-1} to measure shear stress, τ, and steady shear viscosity,

509 $\eta(\dot{\gamma}) = \tau/\dot{\gamma}$. The zero-shear viscosity, η_0 were extracted using the Carreau-Yasuda fitting as,

510 $\eta = \eta_\infty + (\eta_0 - \eta_\infty)\left[1 + \left(t\dot{\gamma}\right)^a\right]^{\frac{m-1}{a}}$, where η_0 is the zero-shear viscosity (mPa·s). Normal

511 stress measurements were additionally carried out in the shear rate range of 10^{-2} to 10^{4} s^{-1},

512 utilising the narrow gap parallel plate method.[66] Note, once the final gap set position was

513 reached, the sample was held until the normal force reached equilibrium (ca. 10 min).

514 **Capillary viscometry.** Polysaccharide solutions were measured for intrinsic viscosity [η]

515 using an Ostwald viscometer ($n = 10$). An Atago DD-7 differential refractometer (Jencons

516 Scientific, UK) was used to estimate polysaccharide concentrations as, $Brix \times 10 \times \frac{\frac{d_n}{d_c}pectin}{\frac{d_n}{d_c}sucrose}$,

517 where $\frac{d_n}{d_c}$ *pectin* and $\frac{d_n}{d_c}$ *sucrose* is 0.146 and 0.149, respectively.

Capillary breakup extensional rheology. Extensional rheology was carried out on a CaBER-1 extensional rheometer (Thermofisher Haake, Germany) equipped with an enclosed measuring unit to minimise evaporation, as described in our earlier study.[67] For all measurements, 76 μL of sample was utilised in the parallel geometry (*diameter*, 6 mm; initial gap and final gap of 3.01 and 9.92 mm, respectively) ($n = 5$). The strike time was 180 ms with a linear stretch profile to avoid filament vibrations during capillary neck thinning. The initial aspect ratio was 1 and at the final aspect ratio was 3.31, correlating to a Hencky strain of 1.19. Surface tensions and density required in relation to the calculations were measured using a PAT1 Profile Analysis Tensiometer (Sinterface Technologies, Germany) and DMA5000 densitometer (Anton Paar, Austria), respectively. Particularly, surface tension was measured using the shape profile of a pendant drop formed at the tip of a capillary in air using the Gauss-Laplace equation.[68] The equation represents a relationship between the curvature of a liquid meniscus and the surface tension (σ_s) as a fitting parameter in, $\sigma_s \left(\frac{1}{r_1} + \frac{1}{r_2} \right) = \Delta p_O + \Delta \rho g z$, where r_1 and r_2 are the radii of curvature, Δp_o is the pressure gradient in a reference plane, $\Delta \rho$ is the density difference, g is the gravity term, and h is the vertical height of the drop measured from the reference plane.

Dynamic light scattering and ζ-potential. The mean hydrodynamic diameter (D_h) and ζ-potential of the polysaccharide solutions were measured on a Nano ZS series Zetasizer (Malvern Instruments, UK) equipped with a 4-mW helium/neon laser at a wavelength output of 633 nm ($n = 6$). ζ-potential were measured using a ZEN1002 Dip cell to achieve a higher field strength and a time delay of 120 s was implemented between measurements to avoid Joule heating.

All-atom Molecular dynamics simulations. A dodecamer chain of repeating segments of *l*-rhamnose and *d*-galacturonic acid was built in *xleap* and *tleap*, as described in a recent NMR

542   study of okra pectin by Liu et. al.[69] Methyl esterification at the C_6 position of galacturonic acid

543   was implemented along the dodecamer. Partial charges of atoms were obtained using

544   semiempirical density functional tight binding (DFTB) (Table S4). Molecular dynamics

545   simulations were performed utilising the Glycam 06j-1 force field for dynamics of

546   carbohydrates and carbohydrate-like molecules in Gromacs 2019.3 compiled with CUDA. The

547   system was solvated in explicit TIP3P water and CHARMM22 glycerol using a triclinic

548   periodic box with a periodic boundary, 1.0 nm. The CHARMM22 forcefield for glycerol is

549   reported to provide experimentally close dynamic diffusion coefficients, however densities are

550   known to deviate by $\leq$ 9%.[70] We observed ca. 1 - 8% deviation in density compared to

551   experimental measurements for $\phi_{0\rightarrow80}$ (Table S2). We also utilised the AMBER forcefield for

552   glycerol, where densities are known to deviate by $\leq$ 4.5%.[70] $\bar{R}$ for $\phi_{0\rightarrow80}$ using AMBER

553   glycerol were in close agreement with the CHARMM22 glycerol results (Figure S8). All

554   simulations started from randomly generated configuration, and a system energy minimisation

555   was carried out for all configurations using the steepest descent algorithm. The Parrinello-

556   Rahman algorithm, the Particle Mesh Ewald method, and the Berendsen thermostat were used

557   for temperature, pressure coupling, and system electrostatics, respectively. Van der Waal's

558   cutoff and Coulomb interactions were both set to 1.2 nm, and simulations were run at 298 K,

559   1 bar of pressure, 4.5×10^{-5} bar of compressibility for 100 ns. Hydrogen bond lengths were

560   constrained using the SHAKE algorithm.

Data availability

562   All data are included in the article and supplementary information. Any additional data are

563   available upon reasonable request.

Declaration of Competing Interest

565 The authors declare that they have no competing financial interests or personal relationships

566 that could have appeared to influence the work reported in this paper.

567 **Acknowledgement**

576

Abbreviations

ϕ_0, okra pectin + water; ϕ_{20}, okra pectin + 20 vol.% glycerol in water; ϕ_{40}, okra pectin + 40 vol.% glycerol in water; ϕ_{60}, okra pectin + 60 vol.% glycerol in water; and ϕ_{80}, okra pectin + 80 vol.% glycerol in water; $\phi_{0 \to 80}$, okra pectin + $0 \to 80$ vol.% glycerol in water; τ, shear stress; $\dot{\gamma}$, shear rate; η, shear viscosity; η_E, extensional viscosity; η_{sp}, specific viscosity; η_0, zero-shear viscosity, η_s, solvent viscosity; η_{sol}, solution viscosity; η_w, water viscosity; $[\eta]$, intrinsic viscosity; η_{red}, reduced specific viscosity; η_{inh}, inherent viscosity; c, concentration; c^*, overlap concentration; c_e, entanglement concentration; λ_E, extensional relaxation time; σ, surface tensions; ρ, density; k_B, Boltzmann constant; MWCO, molecular weight cut-off; M_w, weight-averaged molecular weight; dL, decilitre; R_g, radius of gyration; RMSD, root-mean squared deviations; SEC-MALS, size exclusion chromatography-multi angles light scattering; ATR-FTIR, attenuated total reflectance-Fourier transform infrared spectroscopy; NMR, nuclear magnetic resonance; d, filament diameter; d_0, initial filament diameter; d/d_0, normalised filament diameter; M_c, moisture content; Ψ, normal stress coefficient; x, velocity gradient in fluid; ω, aspect ratio; b, breath of chain; L, length of chain; l_p, persistence length; M_L, mass per unit length; $g(r)$, radial probability distribution; a_w, water activity; σ_N, normal stress; D_h, mean hydrodynamic diameter; r_h, mean hydrodynamic radius; κ^{-1}, Debye length.

28

References

1   Marth, J. D. A unified vision of the building blocks of life. *Nature Cell Biology* **10**, 1015-1015, doi:10.1038/ncb0908-1015 (2008).

2   Berglund, J. *et al.* Wood hemicelluloses exert distinct biomechanical contributions to cellulose fibrillar networks. *Nature Communications* **11**, 4692, doi:10.1038/s41467-020-18390-z (2020).

3   Haas, K. T., Wightman, R., Meyerowitz, E. M. & Peaucelle, A. Pectin homogalacturonan nanofilament expansion drives morphogenesis in plant epidermal cells. *Science* **367**, 1003-1007, doi:10.1126/science.aaz5103 (2020).

4   Sabbadin, F. *et al.* An ancient family of lytic polysaccharide monooxygenases with roles in arthropod development and biomass digestion. *Nature Communications* **9**, 756, doi:10.1038/s41467-018-03142-x (2018).

5   Freund, M. *et al.* The digestive systems of carnivorous plants. *Plant Physiology* **190**, 44-59, doi:10.1093/plphys/kiac232 (2022).

6   Bernal-Bayard, J. *et al.* Bacterial capsular polysaccharides with antibiofilm activity share common biophysical and electrokinetic properties. *Nature Communications* **14**, 2553, doi:10.1038/s41467-023-37925-8 (2023).

7   Justen, A. M. *et al.* Polysaccharide length affects mycobacterial cell shape and antibiotic susceptibility. *Science Advances* **6**, eaba4015, doi:10.1126/sciadv.aba4015 (2020).

8   Drula, E. *et al.* The carbohydrate-active enzyme database: functions and literature. *Nucleic Acids Research* **50**, D571-D577, doi:10.1093/nar/gkab1045 (2022).

9   Zhu, C. *et al.* Rationally designed carbohydrate-occluded epitopes elicit HIV-1 Env-specific antibodies. *Nature Communications* **10**, 948, doi:10.1038/s41467-019-08876-w (2019).

620   10   Hobley, L., Harkins, C., MacPhee, C. E. & Stanley-Wall, N. R. Giving structure to the

621   biofilm matrix: an overview of individual strategies and emerging common themes.

622   *FEMS Microbiology Reviews* **39**, 649-669, doi:10.1093/femsre/fuv015 (2015).

623   11   Wong, S. *et al.* Just add sugar for carbohydrate induced self-assembly of curcumin.

624   *Nature Communications* **10**, 582, doi:10.1038/s41467-019-08402-y (2019).

625   12   Woods, R. J. Predicting the Structures of Glycans, Glycoproteins, and Their

626   Complexes. *Chemical Reviews* **118**, 8005-8024, doi:10.1021/acs.chemrev.8b00032

627   (2018).

628   13   Wu, L. *et al.* Precision native polysaccharides from living polymerization of

629   anhydrosugars. *Nature Chemistry*, doi:10.1038/s41557-023-01193-2 (2023).

630   14   Cao, Y. & Mezzenga, R. Design principles of food gels. *Nature Food* **1**, 106-118,

631   doi:10.1038/s43016-019-0009-x (2020).

632   15   Zhong, C. *et al.* A polysaccharide bioprotonic field-effect transistor. *Nature*

633   *Communications* **2**, 476, doi:10.1038/ncomms1489 (2011).

634   16   Pifferi, C., Fuentes, R. & Fernández-Tejada, A. Natural and synthetic carbohydrate-

635   based vaccine adjuvants and their mechanisms of action. *Nature Reviews Chemistry* **5**,

636   197-216, doi:10.1038/s41570-020-00244-3 (2021).

637   17   Anggara, K. *et al.* Identifying the origin of local flexibility in a carbohydrate polymer.

638   *Proceedings of the National Academy of Sciences* **118**, e2102168118,

639   doi:10.1073/pnas.2102168118 (2021).

640   18   Kaltner, H., Abad-Rodríguez, J., Corfield, A. P., Kopitz, J. & Gabius, H.-J. The sugar

641   code: letters and vocabulary, writers, editors and readers and biosignificance of

642   functional glycan–lectin pairing. *Biochemical Journal* **476**, 2623-2655,

643   doi:10.1042/BCJ20170853 (2019).

644 19 Paulraj, T. *et al.* Primary cell wall inspired micro containers as a step towards a

645 synthetic plant cell. *Nature Communications* **11**, 958, doi:10.1038/s41467-020-14718-

646 x (2020).

647 20 Muthukumar, M. A Perspective on Polyelectrolyte Solutions. *Macromolecules* **50**,

648 9528-9560, doi:10.1021/acs.macromol.7b01929 (2017).

649 21 Alba, K., Bingham, R. J., Gunning, P. A., Wilde, P. J. & Kontogiorgos, V. Pectin

650 Conformation in Solution. *The Journal of Physical Chemistry B* **122**, 7286-7294,

651 doi:10.1021/acs.jpcb.8b04790 (2018).

652 22 Jimenez, L. N., Martínez Narváez, C. D. V. & Sharma, V. Capillary breakup and

653 extensional rheology response of food thickener cellulose gum (NaCMC) in salt-free

654 and excess salt solutions. *Physics of Fluids* **32**, 012113, doi:10.1063/1.5128254 (2020).

655 23 Lopez, C. G., Colby, R. H., Graham, P. & Cabral, J. T. Viscosity and Scaling of

656 Semiflexible Polyelectrolyte NaCMC in Aqueous Salt Solutions. *Macromolecules* **50**,

657 332-338, doi:10.1021/acs.macromol.6b02261 (2017).

658 24 Syryamina, V. N., Wu, X., Boulos, S., Nyström, L. & Yulikov, M. Pulse EPR

659 spectroscopy and molecular modeling reveal the origins of the local heterogeneity of

660 dietary fibers. *Carbohydrate Polymers* **319**, 121167,

661 doi:https://doi.org/10.1016/j.carbpol.2023.121167 (2023).

662 25 Borah, P. K., Rappolt, M., Duary, R. K. & Sarkar, A. Effects of folic acid esterification

663 on the hierarchical structure of amylopectin corn starch. *Food Hydrocolloids* **86**, 162-

664 171, doi:10.1016/j.foodhyd.2018.03.028 (2019).

665 26 Kontogiorgos, V., Margelou, I., Georgiadis, N. & Ritzoulis, C. Rheological

666 characterization of okra pectins. *Food Hydrocolloids* **29**, 356-362,

667 doi:10.1016/j.foodhyd.2012.04.003 (2012).

668   27   Nakagawa, H. & Oyama, T. Molecular Basis of Water Activity in Glycerol–Water

669   Mixtures. *Frontiers in Chemistry* **7**, doi:10.3389/fchem.2019.00731 (2019).

670   28   Marcus, Y. Some thermodynamic and structural aspects of mixtures of glycerol with

671   water. *Physical Chemistry Chemical Physics* **2**, 4891-4896, doi:10.1039/B002966L

672   (2000).

673   29   Zhao, Y. *et al.* A cytosolic NAD+-dependent GPDH from maize (ZmGPDH1) is

674   involved in conferring salt and osmotic stress tolerance. *BMC Plant Biology* **19**, 16,

675   doi:10.1186/s12870-018-1597-6 (2019).

676   30   Raymond, J. A., Morgan-Kiss, R. & Stahl-Rommel, S. Glycerol Is an Osmoprotectant

677   in Two Antarctic Chlamydomonas Species From an Ice-Covered Saline Lake and Is

678   Synthesized by an Unusual Bidomain Enzyme. *Frontiers in Plant Science* **11**,

679   doi:10.3389/fpls.2020.01259 (2020).

680   31   Toxopeus, J., Koštál, V. & Sinclair, B. J. Evidence for non-colligative function of small

681   cryoprotectants in a freeze-tolerant insect. *Proceedings of the Royal Society B:*

682   *Biological Sciences* **286**, 20190050, doi:10.1098/rspb.2019.0050 (2019).

683   32   Yang, L. *et al.* Chemical structure, chain conformation and rheological properties of

684   pectic polysaccharides from soy hulls. *International Journal of Biological*

685   *Macromolecules* **148**, 41-48, doi:10.1016/j.ijbiomac.2020.01.047 (2020).

686   33   Bazunova, M. V., Chernova, V. V., Lazdin, R. Y., Zakharov, V. P. & Kulish, E. I. A

687   Study of the Viscosity Characteristics of Chitosan Solutions in the Presence of Organic

688   Cosolvents. *Russian Journal of Physical Chemistry B* **12**, 1039-1044,

689   doi:10.1134/S1990793118060143 (2018).

690   34   Brunchi, C.-E., Morariu, S. & Bercea, M. Impact of ethanol addition on the behaviour

691   of xanthan gum in aqueous media. *Food Hydrocolloids* **120**, 106928,

692   doi:10.1016/j.foodhyd.2021.106928 (2021).

693   35   Flory, P. J. *Principles of polymer chemistry*. (Cornell university press, 1953).

694   36   De Gennes, P.-G. *Scaling concepts in polymer physics*. (Cornell university press,
695   1979).

696   37   Mukherji, D., Marques, C. M. & Kremer, K. Polymer collapse in miscible good solvents
697   is a generic phenomenon driven by preferential adsorption. *Nature Communications* **5**,
698   4882, doi:10.1038/ncomms5882 (2014).

699   38   Mukherji, D., Marques, C. M., Stuehn, T. & Kremer, K. Depleted depletion drives
700   polymer swelling in poor solvent mixtures. *Nature Communications* **8**, 1374,
701   doi:10.1038/s41467-017-01520-5 (2017).

702   39   Yuan, B., Ritzoulis, C. & Chen, J. Extensional and shear rheology of okra
703   polysaccharides in the presence of artificial saliva. *npj Science of Food* **2**, 20,
704   doi:10.1038/s41538-018-0029-1 (2018).

705   40   Mao, Y. *et al.* Investigating the influence of pectin content and structure on its
706   functionality in bio-flocculant extracted from okra. *Carbohydrate Polymers* **241**,
707   116414, doi:10.1016/j.carbpol.2020.116414 (2020).

708   41   Alba, K., Laws, A. P. & Kontogiorgos, V. Isolation and characterization of acetylated
709   LM-pectins extracted from okra pods. *Food Hydrocolloids* **43**, 726-735,
710   doi:10.1016/j.foodhyd.2014.08.003 (2015).

711   42   Zhu, W. & Obara, H. The pre-shearing effect on the rheological properties of okra
712   mucilage. *Colloids and Surfaces A: Physicochemical and Engineering Aspects* **648**,
713   129257, doi:10.1016/j.colsurfa.2022.129257 (2022).

714   43   Alba, K., Bingham, R. J. & Kontogiorgos, V. Mesoscopic structure of pectin in
715   solution. *Biopolymers* **107**, e23016, doi:10.1002/bip.23016 (2017).

716 44 Nalam, P. C. *et al.* Two-Fluid Model for the Interpretation of Quartz Crystal

717 Microbalance Response: Tuning Properties of Polymer Brushes with Solvent Mixtures.

718 *The Journal of Physical Chemistry C* **117**, 4533-4543, doi:10.1021/jp310811a (2013).

719 45 Antoniou, E. & Alexandridis, P. Polymer conformation in mixed aqueous-polar organic

720 solvents. *European Polymer Journal* **46**, 324-335,

721 doi:10.1016/j.eurpolymj.2009.10.005 (2010).

722 46 Zdunek, A., Pieczywek, P. M. & Cybulska, J. The primary, secondary, and structures

723 of higher levels of pectin polysaccharides. *Comprehensive Reviews in Food Science*

724 *and Food Safety* **20**, 1101-1117, doi:10.1111/1541-4337.12689 (2021).

725 47 Miao, Y., Feher, V. A. & McCammon, J. A. Gaussian Accelerated Molecular

726 Dynamics: Unconstrained Enhanced Sampling and Free Energy Calculation. *Journal*

727 *of Chemical Theory and Computation* **11**, 3584-3595, doi:10.1021/acs.jctc.5b00436

728 (2015).

729 48 Zhang, S. *et al.* Adaptive insertion of a hydrophobic anchor into a poly(ethylene glycol)

730 host for programmable surface functionalization. *Nature Chemistry*,

731 doi:10.1038/s41557-022-01090-0 (2022).

732 49 Bergmann, U. *et al.* Nearest-neighbor oxygen distances in liquid water and ice observed

733 by x-ray Raman based extended x-ray absorption fine structure. *The Journal of*

734 *Chemical Physics* **127**, 174504, doi:10.1063/1.2784123 (2007).

735 50 Jahn, D. A., Wong, J., Bachler, J., Loerting, T. & Giovambattista, N. Glass

736 polymorphism in glycerol–water mixtures: I. A computer simulation study. *Physical*

737 *Chemistry Chemical Physics* **18**, 11042-11057, doi:10.1039/C6CP00075D (2016).

738 51 Dutta, S., Pan, T. & Sing, C. E. Bridging Simulation Length Scales of Bottlebrush

739 Polymers Using a Wormlike Cylinder Model. *Macromolecules* **52**, 4858-4874,

740 doi:10.1021/acs.macromol.9b00363 (2019).

741   52   Oono, Y. & Kohmoto, M. Renormalization group theory of transport properties of

742   polymer solutions. I. Dilute solutions. *The Journal of Chemical Physics* **78**, 520-528,

743   doi:10.1063/1.444477 (1983).

744   53   Pincus, I., Rodger, A. & Prakash, J. R. Viscometric functions and rheo-optical

745   properties of dilute polymer solutions: Comparison of FENE-Fraenkel dumbbells with

746   rodlike models. *Journal of Non-Newtonian Fluid Mechanics* **285**, 104395,

747   doi:10.1016/j.jnnfm.2020.104395 (2020).

748   54   Rivlin, R. S. Normal Stress Coefficient in Solutions of Macromolecules. *Nature* **161**,

749   567-568, doi:10.1038/161567a0 (1948).

750   55   Stelter, M., Brenn, G., Yarin, A. L., Singh, R. P. & Durst, F. Investigation of the

751   elongational behavior of polymer solutions by means of an elongational rheometer.

752   *Journal of Rheology* **46**, 507-527, doi:10.1122/1.1445185 (2002).

753   56   Batchelor, G. K. The stress generated in a non-dilute suspension of elongated particles

754   by pure straining motion. *Journal of Fluid Mechanics* **46**, 813-829,

755   doi:10.1017/S0022112071000879 (1971).

756   57   Shimizu, S. & Matubayasi, N. Preferential Solvation: Dividing Surface vs Excess

757   Numbers. *The Journal of Physical Chemistry B* **118**, 3922-3930,

758   doi:10.1021/jp410567c (2014).

759   58   Ahn, Y., Kim, H. & Kwak, S.-Y. Self-reinforcement of alginate hydrogel via

760   conformational control. *European Polymer Journal* **116**, 480-487,

761   doi:10.1016/j.eurpolymj.2019.03.017 (2019).

762   59   Jimenez, L. N., Martínez Narváez, C. D. V. & Sharma, V. Solvent Properties Influence

763   the Rheology and Pinching Dynamics of Polyelectrolyte Solutions: Thickening the Pot

764   with Glycerol and Cellulose Gum. *Macromolecules* **55**, 8117-8132,

765   doi:10.1021/acs.macromol.2c00170 (2022).

766   60   Nalam, P. C., Ramakrishna, S. N., Espinosa-Marzal, R. M. & Spencer, N. D. Exploring

767   Lubrication Regimes at the Nanoscale: Nanotribological Characterization of Silica and

768   Polymer Brushes in Viscous Solvents. *Langmuir* **29**, 10149-10158,

769   doi:10.1021/la402148b (2013).

770   61   Hiorth, M., Mihailovic, L., Adamczak, M., Goycoolea, F. M. & Sarkar, A. Lubricating

771   Performance of Polymer-Coated Liposomes. *Biotribology* **35-36**, 100239,

772   doi:10.1016/j.biotri.2023.100239 (2023).

773   62   Manrique, G. D. & Lajolo, F. M. FT-IR spectroscopy as a tool for measuring degree of

774   methyl esterification in pectins isolated from ripening papaya fruit. *Postharvest Biology*

775   *and Technology* **25**, 99-107, doi:10.1016/S0925-5214(01)00160-0 (2002).

776   63   Zielinska, S. *et al.* The effect of high humidity hot air impingement blanching on the

777   changes in molecular and rheological characteristics of pectin fractions extracted from

778   okra pods. *Food Hydrocolloids* **123**, 107199, doi:10.1016/j.foodhyd.2021.107199

779   (2022).

780   64   Dinic, J. & Sharma, V. Power Laws Dominate Shear and Extensional Rheology

781   Response and Capillarity-Driven Pinching Dynamics of Entangled Hydroxyethyl

782   Cellulose (HEC) Solutions. *Macromolecules* **53**, 3424-3437,

783   doi:10.1021/acs.macromol.0c00077 (2020).

784   65   Davies, G. A. & Stokes, J. R. On the gap error in parallel plate rheometry that arises

785   from the presence of air when zeroing the gap. *Journal of Rheology* **49**, 919-922,

786   doi:10.1122/1.1942501 (2005).

787   66   Davies, G. A. & Stokes, J. R. Thin film and high shear rheology of multiphase complex

788   fluids. *Journal of Non-Newtonian Fluid Mechanics* **148**, 73-87,

789   doi:10.1016/j.jnnfm.2007.04.013 (2008).

790 67 Li, X., Harding, S. E., Wolf, B. & Yakubov, G. E. Instrumental characterization of

791 xanthan gum and scleroglucan solutions: Comparison of rotational rheometry, capillary

792 breakup extensional rheometry and soft-contact tribology. *Food Hydrocolloids* **130**,

793 107681, doi:10.1016/j.foodhyd.2022.107681 (2022).

794 68 Derkach, S. R., Krägel, J. & Miller, R. Methods of measuring rheological properties of

795 interfacial layers (Experimental methods of 2D rheology). *Colloid Journal* **71**, 1-17,

796 doi:10.1134/S1061933X09010013 (2009).

797 69 Liu, J. *et al.* Structure characterisation of polysaccharides in vegetable "okra" and

798 evaluation of hypoglycemic activity. *Food Chemistry* **242**, 211-216,

799 doi:10.1016/j.foodchem.2017.09.051 (2018).

800 70 Jahn, D. A., Akinkunmi, F. O. & Giovambattista, N. Effects of Temperature on the

801 Properties of Glycerol: A Computer Simulation Study of Five Different Force Fields.

802 *The Journal of Physical Chemistry B* **118**, 11284-11294, doi:10.1021/jp5059098

803 (2014).

804

Supplementary Files

This is a list of supplementary files associated with this preprint. Click to download.

- SupportingInfoOkraPaper27102023PKBGY.docx